Journal of the Korean Physical Society, Vol. 77, No. 7, October 2020, pp. 605∼612

Implementation of a Sinusoidal Raster Scan for High-Speed Atomic Force Microscopy

Luke Oduor Otieno and Yong Joong Lee*
School of Mechanical Engineering, Kyungpook National University, Daegu 41566, Korea

Bernard Ouma Alunda
School of Mines and Engineering, Taita Taveta University, P.O. Box 635-80300, Voi, Kenya

(Received 13 May 2020; revised 18 June 2020; accepted 18 June 2020)

To improve the speed of an atomic force microscope (AFM), one must improve the bandwidth of its components, and the lateral XY scanner is no exception. Sinusoidal raster scans provide a simple way of improving lateral scan rates without the need for additional hardware and/or complex control algorithms. However, a raster scan using a sinusoidal waveform leads to a non-uniform probe-sample velocity. Uniform spatial sampling of scan data can be achieved in this case by varying the sampling rate as the probe sample velocity varies. In this work, we present a field-programmable gate array (FPGA)-based implementation of a sinusoidal raster scan with uniform spatial sampling for a high-speed atomic force microscope (HS-AFM). Using a home-made HS-AFM scanner and a custom controller, we demonstrate the performance of our approach by imaging Blu-ray disk data tracks in the contact mode. While the results show images comparable to those acquired using the traditional triangular raster scans, mirroring effects are better suppressed in high-speed imaging with sinusoidal scan signals.

Keywords: High-speed atomic force microscopy, Sinusoidal raster scan, FPGA
DOI: 10.3938/jkps.77.605

I. INTRODUCTION

The past two and a half decades have seen much progress in the development of high-speed atomic force microscopy (HS-AFM). State-of-the-art HS-AFMs are now capable of acquiring 100 pixels × 100 pixels images at a rate of 10 to 20 frames per second [1]. The imaging rate of an atomic force microscope is generally limited by the bandwidth of its individual components. Among these components are the scanning probe, the lateral and vertical scanners, the vertical feedback controller, and the data acquisition system. The limitations have been detailed by Fleming [2] and the references therein.

As a way to improve the imaging rate of AFMs, the bandwidth of at least one of the speed-limiting components is commonly increased. One such component is the XY scanner. Conventionally, an AFM acquires images by using triangular positioning signals to scan a sample one line at a time in a raster scan pattern. The lateral XY scanner has to track the positioning signal within acceptable error limits, and as such, the scanning rates are limited to a maximum of between 1% and 10% of the lateral scanner bandwidth when using triangular signals [3]. Limiting the line rate in this manner has two effects: the likelihood of exciting the resonant modes of a scanner is reduced and sufficient harmonics of the triangular positioning signal are accommodated to reduce the tracking error to within acceptable limits for most scanning applications. The downside of this approach is the limited achievable scanning rates for any given scanner.

One of the approaches used to improve line rates is redesigning lateral scanners to improve their mechanical bandwidths [4,5]. This can be achieved by reducing the mass of the central moving sample stage or increasing the stiffness of the flexure scanner. The former limits the sample size that can be mounted on the sample stage while the latter reduces the achievable scan range. Both approaches lead to a difficulty in scanning large samples. Another approach is the implementation of control algorithms in order to compensate for unwanted vibrations in addition to reducing the magnitude of the first resonant peak of the scanner [3, 6]. However, such fixes are often complex to implement, requiring additional position sensors to track the displacement of the scanner. Additionally, because the components of triangular waveforms beyond the bandwidth of the scanner are distorted in phase and amplitude, error in tracking the positioning signal increases as the scan rate increases [7].

Approaches that are simpler to implement generally

*E-mail: yjlee76@knu.ac.kr

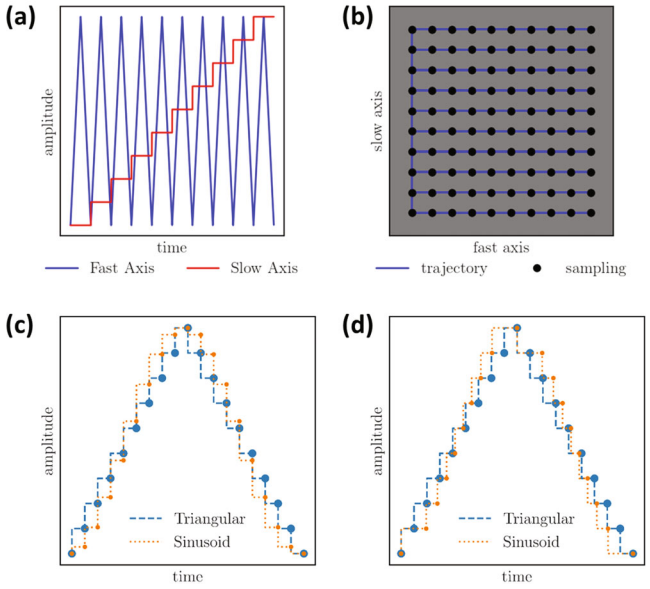

Fig. 1. Raster scan for an image size of 10 pixels by 10 pixels. (a) Fast axis and slow axis signals. (b) Raster showing probe trajectory (blue) and sampling points (black). (c) Triangular and sinusoidal scan signals with a uniform sampling rate in time. (d) Sinusoidal and triangular scan signals uniformly sampled in amplitude.

involve reducing the harmonic contents of the scan signal. This has been demonstrated through the shaping of triangular scan signals to remove the sharp vertices [4,7, 8]. The shaping of triangular waveforms is of particular interest in applications where a constant sample-probe velocity needs to be maintained. However, the harmonic content of the shaped waveforms still remains significant. In the case of optimal scan waveforms, the penalty of increasing the scan rate is a much reduced scan range [7].

A straightforward method of improving the open-loop performance of scanners is to use sinusoids [2,9]. Pure sinusoids can be used to scan at and even beyond the resonance frequency of a scanner [9,10] because the risk of a harmonic exciting an undesired resonance mode of the scanner is negligible. Additionally, sinusoids are used in non-raster scans to improve frame acquisition rates [11–13]. However, because the probe-sample velocity varies when using sinusoids, uniform spatial sampling is not possible with a constant sampling rate. Most implementations of this scan method acquire data at fixed temporal sampling rates and then interpolate the acquired data to a uniform grid, line by line [7,9,10]. This adds a layer of processing and estimating to the measurement process. Uniform spatial sampling can be achieved by varying the sampling rate as the probe-sample velocity varies. Direct digital synthesis (DDS) of sinusoidal scan signals by varying the time between samples as the phase of the synthesized waveform varies can be implemented in a scan engine to achieve this without altering other components of the scan engine or the hardware.

In this work, the implementation of a sinusoidal raster scan with uniform spatial sampling for a HS-AFM is presented. Field-programmable gate array (FPGA) hardware is used to synthesize the scan signal by varying the delay between the output samples of the synthesized scan waveform. A non-uniform update rate is the only added modification to a conventional triangular scan signals generator. A FPGA is selected for this implementation because the technology is becoming fairly widespread in real-time applications and it provides deterministic timing at the resolution of its clock period. Additionally, a number of commercial and custom HS-AFM controllers have been designed using FPGAs [8]. The harmonics of the generated waveforms are compared to those of conventional triangular raster scan signals. Further, we demonstrate the effectiveness of the proposed approach by scanning data tracks of a Blu-ray disk in the contact mode and by comparing the results with those obtained using triangular scan signals.

II. SINUSOIDAL RASTER SCAN

For raster scans, the fast axis of the lateral scanner is supplied with a scan signal whose frequency equals the required line rate. The slow axis is supplied with a staircase waveform to enable movement from one line to the other. This approach facilitates the uniform spatial sampling of the scanned area along both axes at a uniform sampling rate. An illustration of this is shown in Fig. 1. Figure 1(a) shows the signals applied to the two lateral axes while Fig. 1(b) shows the trajectory traced by the probe on the sampled surface. Figure 1(c) shows triangular and sinusoidal staircase waveforms that are uniformly sampled in time. Amplitude levels representing the stairs differ. Figure 1(d) shows triangular and sinusoidal staircase waveforms that sample the scanned space uniformly. If a uniform spatial sampling is to be achieved the sampling rate during sinusoidal scans must vary as the probe-sample speed varies. The signals in Fig. 1(c) and Fig. 1(d) appear as they are constructed within the FPGA. A low-pass filter can be used at the output of the digital-to-analog converter to reduce the effect of the steps [14].

1. Constructing a Sinusoidal Scan Signal

The adopted approach was to sequentially move the scanner from one sampling point to the next along the scan trajectory. For a scan of width 2R scanned at a line rate of f Hz, a single period of the triangular and the

sinusoidal scan signals can be expressed, respectively, as

$$x_{\text{tri}}(t) = \begin{cases} -R + 4Rft, & \text{if } 0 \le t \le \frac{T}{2} \\ R - 4Rf\left(t - \frac{T}{2}\right), & \text{if } \frac{T}{2} \le t \le T \end{cases} \quad (1)$$

$$x_{\text{sin}}(t) = -R\cos(2\pi ft) \quad (2)$$

where $T = 1/f$ is the period of the waveform.

A total of $2N-1$ steps are required for a cycle to implement the triangular waveform in staircase form with N steps per half cycle. Designating the step number using k and substituting the kT_s for t, where the sampling period $T_s = T/(2N-2)$, the discretized form of Eq. (1) becomes

$$x_{\text{tri}}(kT_s) = \begin{cases} -R + k\Delta, & \text{if } 0 \le k \le N-1 \\ 3R - k\Delta, & \text{if } N \le k \le 2N-2, \end{cases} \quad (3)$$

where the value $\Delta = 4R/(2N-2)$ is the step size. Simple sequential additions and subtractions can be used to implement the waveform as shown in the equation below by maintaining a constant delay of T_s between the samples:

$$x_k = \begin{cases} -R, & \text{if k} = 0 \\ x_{k-1} + \Delta, & \text{if } 1 \le k \le N-1 \\ x_{k-1} - \Delta, & \text{if } N \le k \le 2N-2 \end{cases} \quad (4)$$

Figure 1(d) essentially shows that Eq. (4) can be used to synthesize a sinusoidal raster scan signal by varying the step durations as the amplitude of the signal varies. For equal sampling in amplitude, time becomes the subject of Eq. (2). The time instant corresponding to the beginning of each of the staircase levels for a sinusoidal scan signal can be expressed as

$$t_k = \frac{\cos^{-1}(-\frac{x_k}{R})}{2\pi f} \quad (5)$$

by simply making t the subject of the expression in Eq. (2). During the implementation, the values of t_k can be precomputed and stored in a lookup table (LUT) to reduce the amount of resources required to compute the expression in the FPGA.

2. Implementation

The scan signal was implemented using a multifunction reconfigurable input/output (RIO) device with a user-programmable FPGA on board (NI PXI-7851R, National Instruments, USA). It has a maximum update rate of 1 MSa/s and a maximum sampling rate of 750 kSa/s. To make the implementation simple, we used a LUT to hold pre-computed values of Eq. (5) at $f = 1$ Hz and with $R = 1$. The length L of the lookup table is selected to be longer than the maximum pixel size typically used for a line during the scans.

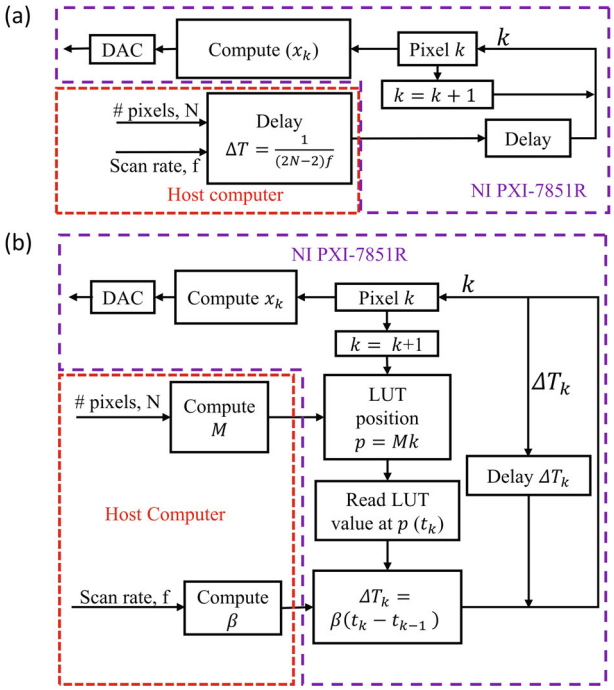

Fig. 2. Block diagram of the implementation: (a) triangular scan waveforms and (b) sinusoidal scan waveforms.

Typically, a LUT-based direct digital synthesis (DDS) produces samples at a constant clock rate. In a such case, the output frequency is varied by undersampling the values in the LUT while the amplitude is varied by scaling. In our case, the amplitude varies in fixed step sizes while the output update rate varies nonuniformly in time to produce a sinusoidal waveform. Further requirements for a typical AFM scan signal generator include a provision for arbitrary settings for scan frequencies and scan resolutions. Because the t_k values in the LUT are computed for $f_{\text{ref}} = 1$ Hz, multiplying the values read from the LUT with the ratio f_{ref}/f scales the sampling time to achieve a variation in the scan rate. If the current time value from the lookup table is t_k and the next time value from the table is t_{k+1}, the delay δt_k between the current and the next amplitude level is given by

$$\delta t_k = \beta\,(t_{k+1} - t_k)\,, \quad (6)$$

where $\beta = f_{\text{ref}}/f$ is the ratio between the reference frequency for the LUT values f_{ref} and the desired line rate f.

In a raster scan scheme where the sampling rate is governed by the number of pixels in a line, increasing the resolution of the scan at a fixed line frequency corresponds to an increase in the sampling rate. For the sinusoidal raster scan implementation discussed in this work, the increase in the sampling rate is achieved by undersampling or oversampling the values contained in the LUT. The approximation of the number of positions,

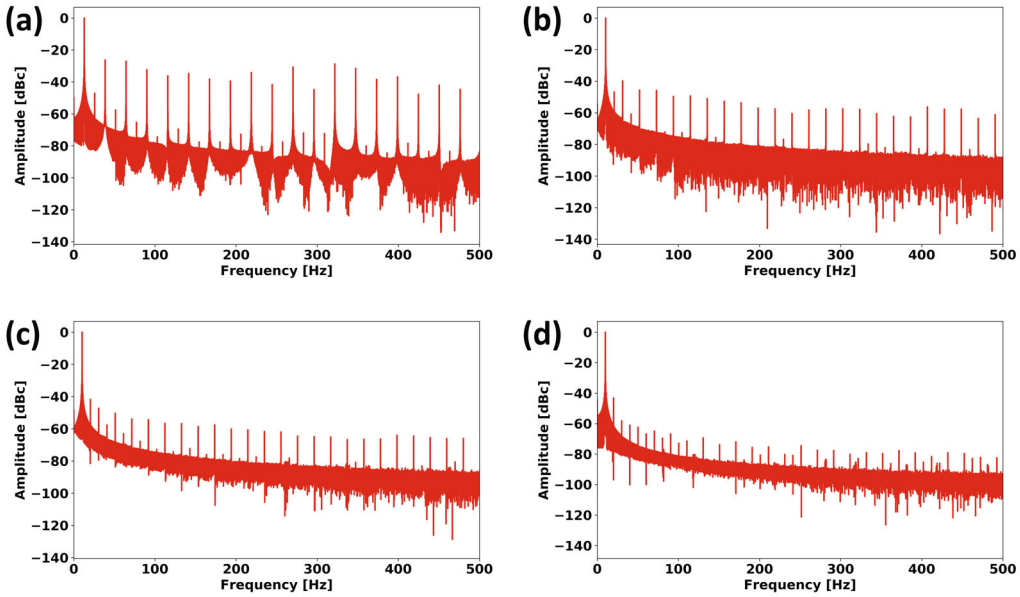

Fig. 3. Spectra of the implemented sinusoidal raster scan signal at 10 Hz. The spectra are obtained for (a) $N = 10$, (b) $N = 50$, (c) $N = 100$, and (d) $N = 512$. The purity of the generated scan signal improves with increasing value of N.

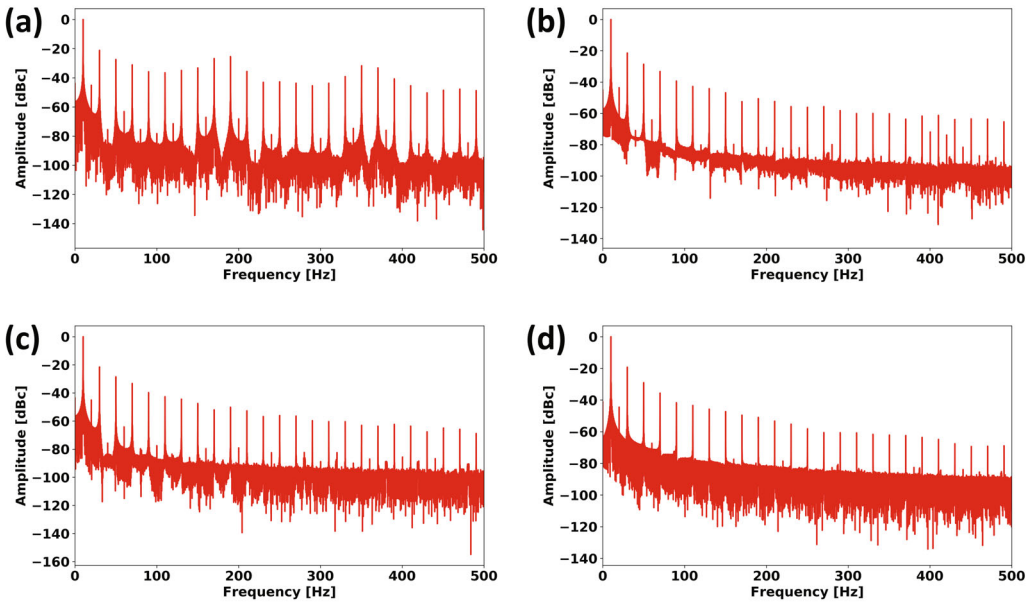

Fig. 4. Spectra of the implemented triangular raster scan signal at 10 Hz. The spectra are obtained for (a) $N = 10$, (b) $N = 50$, (c) $N = 100$, and (d) $N = 512$. As the value of N is increased, the approximation errors decrease while the harmonics of the triangular waveform remain prominent.

M, to be skipped in the LUT between successive sampling points is given by the integer number in

$$M = \left\lfloor \frac{L}{2N-2} \right\rfloor , \tag{7}$$

where the floor notation, $\lfloor\ \rfloor$, represents a rounding down. Rounding down keeps the computed positions within the size of the LUT. To sample the elements of the LUT, we use a 32-bit accumulator and interpolation to improve the estimates of time.

Figures 2(a) and (b) show implementations of triangular and sinusoidal raster scan signals, respectively. The pixel number corresponds to a signal amplitude level, which is computed by addition, as shown in Eq. (4). Because the delay between the output signal amplitude levels is constant for a triangular raster scan signal, the im-

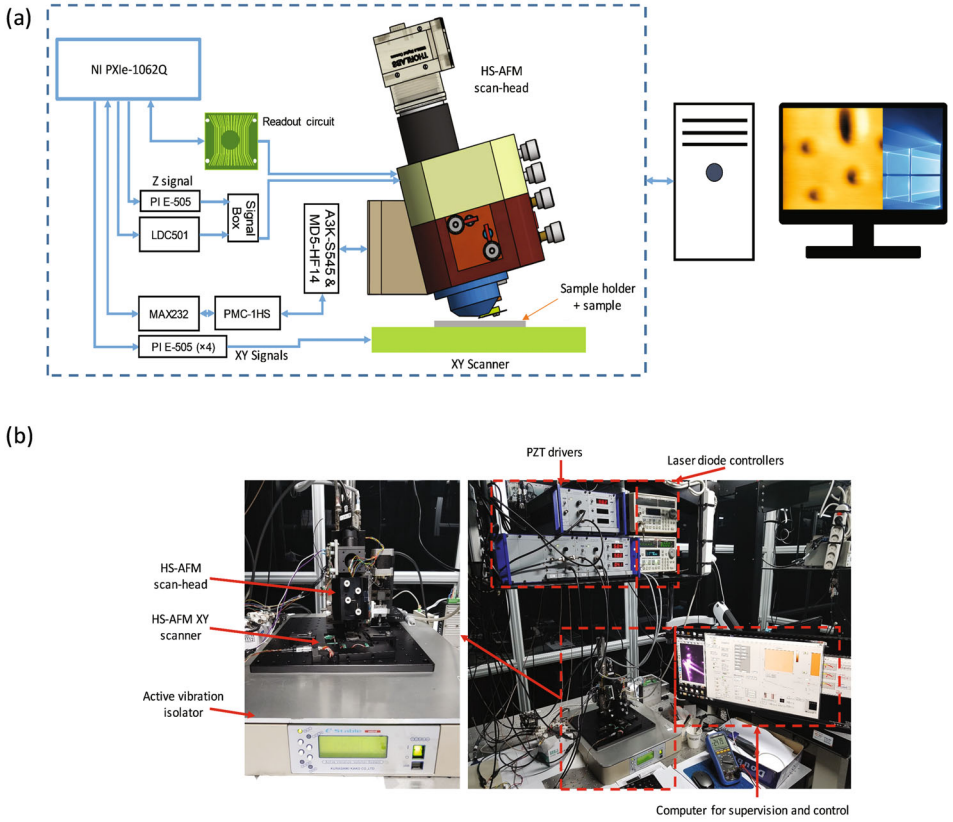

Fig. 5. (a) Schematic showing the connections between the HS-AFM head and the controller, and (b) a photograph of the experimental setup.

plementation is straightforward. Each iteration involves computing a signal level and waiting for the next sampling instant. For a sinusoidal scan signal, the delay between signal levels depends on the phase of the waveform. The values M and T are pre-computed in the host computer for every new value of the resolution N and the scan rate f, respectively. For this implementation, the LUT size is $L = 4096$. The timing resolution is 25 ns because the clock rate of our FPGA hardware is 40 MHz. An improved temporal resolution can be achieved by using a faster clock rate. After every trace/retrace cycle, the LUT position is re-initialized for the next cycle.

3. Implementation Results

After the implementation, 10-Hz waveforms are generated at different resolutions. To compute the spectra of the DDS-generated waveforms, the waveforms are sampled with an analog-to-digital converter (ADC) running at 100 kSa/s for 20 s. The results are shown in Figs. 3(a) through (d). In Fig. 3(a), $N = 10$. The DDS-generated signal has a significant number of harmonics just under 10 times smaller than the desired signal frequency. In Fig. 3(b), N is increased to 100. The largest harmonic

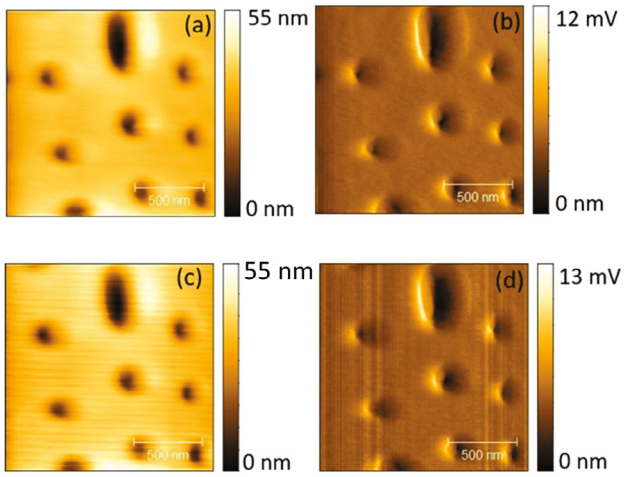

Fig. 6. Blue ray disk images acquired at 20 Hz. (a) and (c) show the topography while (b) and (d) show the error signals. Triangular scan signals are used to acquire the top images while sinusoidal scan signals are used to acquire the bottom images. The scan size is 1.5 µm × 1.5 µm.

is at least 100 times smaller than the desired signal. As N is increased further to 200 in Fig. 3(c) and 512 in Fig. 3(d), the undesired frequency components in the

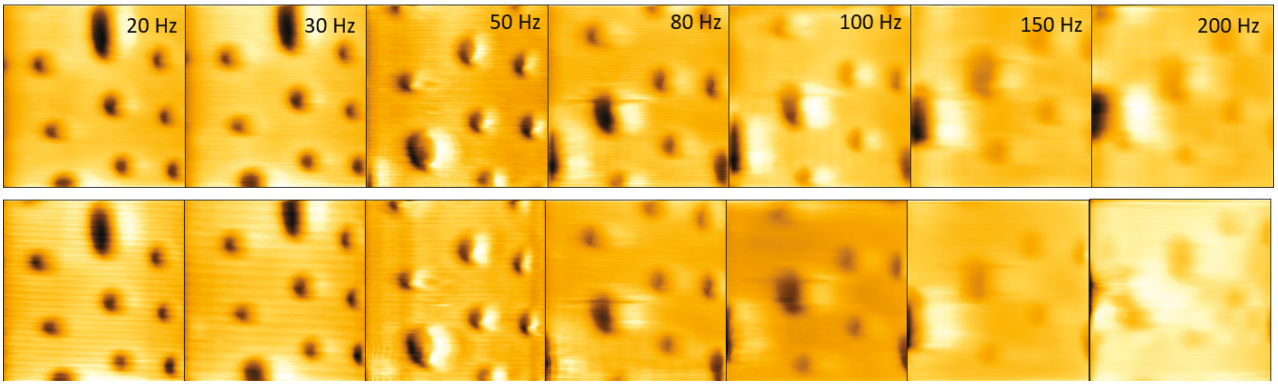

Fig. 7. Topographical images of a Blu-ray disc. Each vertical pair contains images acquired using triangular (top) and sinusoidal (bottom) raster scans. The imaging rates in Hz are indicated in the top right of each image in the top row. The scan size is 1.5 μm × 1.5 μm.

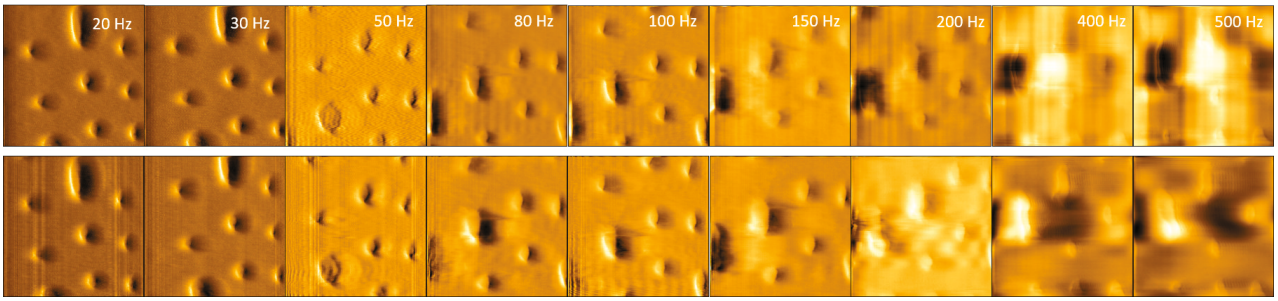

Fig. 8. Error images of a Blu-ray disc. Each vertical pair contains images acquired using triangular (top) and sinusoidal (bottom) raster scans. The imaging rates in Hz are indicated in the top right of each image in the top row. The scan size is 1.5 μm × 1.5 μm.

DDS-generated signal are reduced further. Increasing N leads to smaller step sizes and consequent improvements in the estimate of the signal amplitude. Because acquiring AFM images at resolutions of 100 pixels × 100 pixels or higher is typical, the poor quality signals generated at very low values of N should not hinder the application of this method in typical AFM image acquisitions.

In comparison, triangular raster scan signals constructed using a similar method yield the results shown in Figs. 4(a) through (d) for N values of 10, 50, 100 and 512, respectively. At low values of N, the spectra of the triangular and the sinusoidal scan waveforms are comparable. Figure 3(a) and Fig. 4(a) illustrate this. However, as the value of N increases progressively, as shown in Figs. 3(b) through (d) and Figs. 4(b) through (d), the approximation errors are reduced in the sinusoidal and triangular approximations while the harmonics of the triangular approximation remain prominent.

The maximum achievable frequency for the sinusoidal waveforms synthesized by varying the DDS update rate is limited to about 63.69% of the maximum achievable frequency for a triangular waveform synthesized in a similar manner. Beyond this value, the spectral purity of the waveforms produced using the sinusoidal raster scan approach described in this work starts deteriorating because the waveforms produced no-longer approximate sinusoids because the maximum lateral probe-sample speed for a sinusoidal waveform is about $\pi/2$ of the probe-sample speed for a triangular waveform of the same frequency [11]. The implication of this difference on the maximum achievable lateral scan rate is as follows. While sampling at a maximum rate of 750 kSa/s, the NI-7851R-based AFM controller described in this work can acquire a maximum of approximately 38 100 pixel × 100 pixel trace and retrace frames per second (fps) when using the triangular raster scan method described in this work. However, the maximum achievable rate using sinusoidal scan signals constructed using the method described in this work is approximately 24 fps. Faster digital-to-analog conversion (DAC) hardware is required to improve the acquisition rates.

III. IMAGING

The experimental setup is shown in Fig. 5. The setup consists of a custom HS-AFM scan-head, a custom HS-AFM XY scanner and a custom HS-AFM controller. The chassis (PXIe-1062Q, National Instruments, USA) contains a real-time controller and a PXI-7851R RIO card, within which the scan-signal generator is implemented.

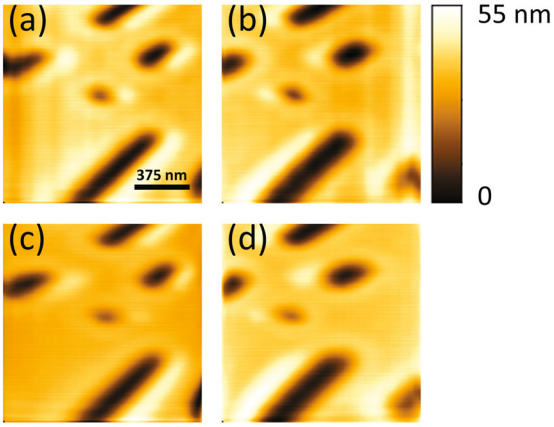

Fig. 9. Topographical images of a Blu-ray disc acquired at 100 Hz. The scan size is 1.5 μm × 1.5 μm and the pixel size is 100 × 100. Trace images are shown in (a) and (c) while the retrace images are shown in (b) and (d). Each vertical pair contains images acquired using triangular (top) and sinusoidal (bottom) raster scans. Mirroring of the features occurs near the left and the right edges of the images in (a) and (b).

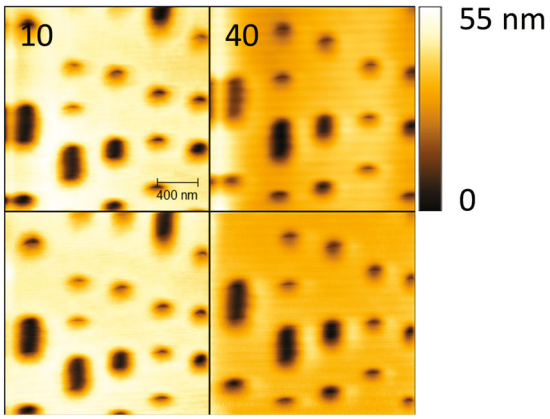

Fig. 10. Topographical images of a Blu-ray disc. The scan size is 2.5 μm × 2.5 μm. Each vertical pair contains images acquired using triangular (top) and sinusoidal (bottom) raster scans. Mirroring of the features occurs near the left edge of the trace images acquired using a triangular raster scan. The imaging rates in Hz are indicated in the top left of each image in the top row.

Piezo drivers (E-505, Physik Instrumente, Germany) are used to drive the XY and the Z scanners. A computer hosts a custom LabVIEW-based HS-AFM control program.

Imaging experiments were carried out in the contact mode. The sample was a piece of a Blu-ray disk. In the first experiment, for a scan area of approximately 1.5 μm × 1.5 μm, images were acquired at increasing speeds by using triangular and sinusoidal scan signals. The resolution was set at 256 pixels × 256 pixels. The images acquired at 20 Hz are shown in Fig. 6. The feedback controller parameters required slight adjustment while using sinusoidal scan signals because of the increased maximum tip-sample velocity. The images acquired using sinusoidal raster and triangular raster scans are of comparable clarity.

When the speed is varied, the system tracks topography up to around 200 Hz. The images obtained using both triangular and sinusoidal raster scan signals are comparable, as shown in Fig. 7. When the speed is further increased, the error images show features clearer than the topography signals. This is indicative of limitations in the vertical feedback bandwidth [15]. In our setup, the Z scanner piezo-amplifier is the limiting element in the overall vertical control loop. We varied the scan rate up to 500 Hz, as shown in Fig. 8. Beyond 200 Hz, the error images obtained using the sinusoidal raster scan appear to be clearer than those obtained using the triangular raster scan.

Another benefit of the sinusoidal raster scan is that because of the reduced probe sample velocity near the edge of the scan, the effect of inertia, which leads to mirroring the features near the edges of the trace and retrace scan images is not as pronounced as it is in triangular raster scans [16]. Figures 9(a) and (b) show mirroring in the left of the trace image and the right of the retrace image when using a triangular raster scan. The effect is barely visible in Figs. 9(c) and (d), which were acquired using a sinusoidal raster scan. Figure 10 shows that mirror images of the features close to the left edge become more prominent with increasing scan rate. The effect is clear in triangular raster scan images, but is barely visible in sinusoidal raster scan images. Scan speeds have to be limited to levels that avoid excessive mirroring.

IV. CONCLUSION

We have presented a simple implementation of sinusoidal raster scan for a HS-AFM. The approach uses a non-uniform update rate to acquire a uniformly sampled image. Estimates of the desired scan waveforms improve with increasing pixel size of the image to be acquired. The approach presented in this work may be useful in HS-AFM controllers with limited DAC update rates and/or limited ADC sampling rates.

ACKNOWLEDGMENTS

This work is supported by the Basic Science Research Program through the National Reasearch Foundation of Korea (NRF) funded by the Ministry of Science and ICT (2018R1A2B6008264).

REFERENCES

[1] T. Ando, Biophys. Rev. **10**, 285 (2018).
[2] A. J. Fleming, Ultramicroscopy **110**, 1205 (2010).
[3] D. Croft, G. Shed and S. Devasia, J. Dyn. Syst. Meas. Control **123**, 35 (2001).
[4] G. Schitter *et al.*, IEEE Trans. Control Syst. Technol. **15**, 906 (2007).
[5] K. Miyata *et al.*, Rev. Sci. Instrum. **84**, 043705 (2013).
[6] H. Habibullah, H. R. Pota and I. R. Petersen, Sens. Actuators A **292**, 137 (2019).
[7] A. J. Fleming and A. G. Willis, IEEE Trans. Control Syst. Technol. **17**, 552 (2009).
[8] A. P. Nievergelt *et al.*, in *2017 IEEE International Conference on Advanced Intelligent Mechatronics (AIM)*, (Munich, Germany, 2017), p. 731.
[9] A. D. L. Humphris, M. J. Miles and J. K. Hobbs, Appl. Phys. Lett. **86**, 034106 (2005).
[10] L. M. Picco *et al.*, Nanotechnology **18**, 044030 (2006).
[11] Y. R. Teo, Y. Yong and A. J. Fleming, Asian J. Control **20**, 1352 (2018).
[12] S. K. Das *et al.*, IEEE Access **7**, 115603 (2019).
[13] N. Nikooienejad, M. Maroufi and S. O. R. Moheimani, Rev. Sci. Instrum. **90**, 073702 (2019).
[14] G. E. Fantner *et al.*, Rev. Sci. Instrum. **76**, 026118 (2005).
[15] P. K. Hansma, G. Schitter, G. E. Fantner and C. Prater, Science **314**, 601 (2006).
[16] T. Ando *et al.*, Jpn. J. Appl. Phys. **41**, 4851 (2002).